Peer-reviewed version available at *Micromachines* **2020**, *11*, 256; doi:10.3390/mi11030256

Article

Black Metals: Optical Absorbers

Stefan Lundgaard[1,2,*], Soon Hock Ng[1,2], Yoshiaki Nishijima[3,4], Michael Mazilu[5,*], Saulius Juodkazis[1,4,6]

1 Optical Sciences Centre and ARC Training Centre in Surface Engineering for Advanced Materials (SEAM), School of Science, Swinburne University of Technology, Hawthorn, VIC 3122, Australia
2 Melbourne Centre for Nanofabrication, the Victorian Node of the Australian National Fabrication Facility, 151 Wellington Rd., Clayton 3168 VIC, Australia
3 Department of Electrical and Computer Engineering, Graduate School of Engineering, Yokohama National University, 79-5 Tokiwadai, Hodogaya-ku, Yokohama 240-8501, Japan
4 Institute of Advanced Sciences, Yokohama National University, 79-5 Tokiwadai, Hodogaya-ku, Yokohama 240-8501, Japan
5 SUPA, School of Physics and Astronomy, University of St. Andrews, St. Andrews, KY16 9SS, Scotland
6 Tokyo Tech World Research Hub Initiative (WRHI), School of Materials and Chemical Technology, Tokyo Institute of Technology, 2-12-1, Ookayama, Meguro-ku, Tokyo 152-8550, Japan
* Correspondence: (S.L.) slundgaard@swin.edu.au; (M.M) michael.mazilu@st-andrews.ac.uk

Abstract: We demonstrate a concept and fabrication of lithography-free layered metal-SiO_2 thin-film structures which have reduced reflectivity (black appearance), to as low as 0.9 %, with 4.9 % broadband reflectance (8.9 % for soda lime) in the 500 - 1400 nm range. The multi-layered (four layers) thin-film metamaterial is designed so that optical impedance matching produces minimal reflectance and transmittance within the visible and infra-red (IR) spectral region for a range of incident angles. The structure has enhanced absorbance and is easily tuned for reduced minimal transmission and reflection.

Keywords: Metamateraial; optical absorber; thin-film optics

1. Introduction

Photonic metamaterials are providing new capabilities for highly efficient and tunable solutions in photonic devices with light phase delay and intensity modulation for resonators, waveguides, absorbers, switches and detectors [1–3]. Perfect absorbers are of interest within the metamaterial family due to wavelength specific applications such as solar cells, photo-detectors and optical filters. Meta-materials/surfaces have sub-wavelength scale films/structures and can create unusual optical properties, e.g., left-handed (negative refractive index) materials [4]. By tailoring real and imaginary parts of the refractive index, a new field of topological photonics has emerged where breaking optical reciprocity and parity-time symmetry is achieved [5,6]. Recently, modeling and fabrication of metasurfaces with designed amplitude and phase delay patterns can be done using open access software which outputs design files required for popular e-beam or projection lithographies [7].

Devices and structures modulating and manipulating waves can be made for sound, light and electrical waves [8–10]. In particular, impedance matching is a method of preventing wave reflection, a technique used heavily in electronics. Metamaterials and thin-film technology has made it possible for the impedance of fabricated devices to match the impedance of bands in the electromagnetic spectrum [11,12]. Negative refractive index materials in the optical spectrum have previously been realised through lithography and thin-film deposition within the optical spectrum [13]. Now, a novel approach is required for simple minimal-layer films to realise impedance matching in the optical domain of the electromagnetic spectrum.

Here, we use a lithography-free multi-layer approach to fabricate perfect absorbers by impedance matching principle for light in the visible range [11]. The streamlined and simple fabrication process reduces time and cost over standard lithography-based approaches. Thin film techniques allow for these metamaterials to be designed at sub-wavelength thicknesses, creating highly optimised structures for a particular spectral range. By changing nano-film material and thickness, colors are produced and particular wavelength bands are selectively reflected. Appearance of color is a consequence of the optical impedance mismatching at different wavelengths.

Peer-reviewed version available at Micromachines 2020, 11, 256; doi:10.3390/mi11030256

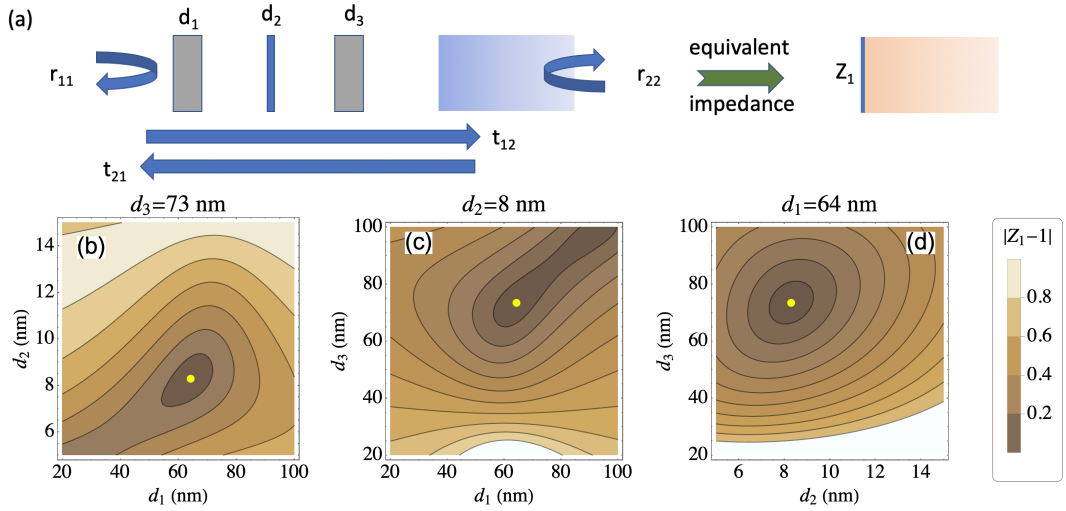

Figure 1. (a) Schematic representation of the structure consisting of three layers (silica, metal, silica) with respective thicknesses (d_1, d_2 and d_3) on top of the thick metal layer. The field coefficients are defined in the text. (b-d) Impedance mismatch $|Z_1 - 1|$ as a function of the different layer thicknesses for normal incidence at a wavelength ($\lambda = 500$ nm). The yellow dot corresponds to the layer thicknesses ($d_1 = 64$ nm, $d_2 = 8$ nm, $d_3 = 73$ nm) minimising overall back-reflection r_{11}.

2. Theory

The optical absorbers consist of a simple stacked layer of dielectric-metal-dielectric on a metal mirror (Figs. 1, 2(a)). Layer thicknesses are optimised through the help of simulations in Matlab (MathWorks, Natick, MA USA) which determines the optical impedance of the sub-wavelength thin-films. The optical absorbers are then fabricated via standard thin film deposition techniques. Using different materials for d_2 creates a change in impedance of the absorber and hence color (Figure. 2(b)).

A scattering matrix is used in conjunction with material permittivity and permeability properties to determine effective zero reflection $R = 0$. This zero reflection regime is realised when the layers create an effective impedance that matches the impedance of air on the incident side. This interface impedance corresponds to the image impedance defined in reference [11] as:

$$Z_1 = \sqrt{\frac{(r_{22}r_{11} - r_{11} - r_{22} - t_{12}t_{21} + 1)\,(r_{22}r_{11} + r_{11} - r_{22} - t_{12}t_{21} - 1)}{(r_{22}r_{11} - r_{11} + r_{22} - t_{12}t_{21} - 1)\,(r_{22}r_{11} + r_{11} + r_{22} - t_{12}t_{21} + 1)}}. \quad (1)$$

where the field transmission (t_{12}, t_{21}), and reflection (r_{11}, r_{22}) coefficients (represented in Figure. 1) are calculated to take into account the whole structure from the first air-silica interface to the final silica-metal interface.

The layer thicknesses are sub-wavelength which allows for an incident wave to perceive the material as having a different impedance than that of the individual materials used. Calculations were performed for low reflectivity and larger angular range down to the Brewster angle using method described in ref. [11]. Refractive index of the materials were taken from the public database [14] or the popular finite difference time domain (FDTD) program Lumerical (Lumerical Inc., Vancouver, BC Canada) as indicated where applies.

Reflection spectra are calculated by stepped iterations across the visible spectrum and layer thicknesses. The wavelength is in stepped intervals of 1 nm from 300 - 1000 nm, thickness steps for d_1 are 1 nm, d_2 0.5 nm and d_3 1 nm intervals. Spectral plots and surface contour maps for visualisation are realised and material layer thicknesses are then extrapolated for zero reflectance $R = 0$.

Peer-reviewed version available at Micromachines 2020, 11, 256; doi:10.3390/mi11030256

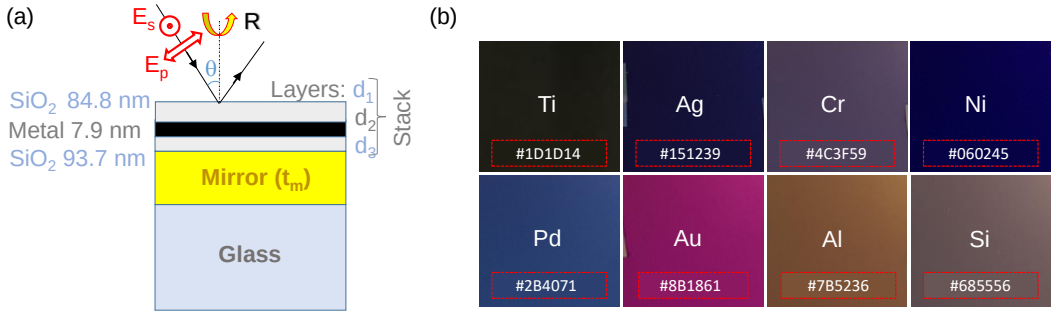

Figure 2. Black metals. (a) Schematic of the structure of stacked nano-films [11] investigated for absorbance control; the numerically optimised thicknesses for black-Ti are shown (see Section. 4.1 for details). (b) Photos of reflected colours under fluorescent white light illumination for various materials in the layer two (d_2). Hexadecimal colour codes with the respective colours are shown on the images. The samples are all fabricated with the same target thicknesses for all layers: layer-1 $d_1 = 84.8$ nm, layer-2 $d_2 = 7.9$ nm, layer-3 $d_3 = 93.7$ nm. Thickness of the back Ti mirror was $d_m = 100$ nm.

3. Experimental

3.1. Fabrication

Soda lime substrates of 1 mm thickness with thin films of metal and SiO_2 were fabricated to produce the optical absorbers. The films were deposited using an *AXXIS* physical vapour deposition (PVD) chamber (Kurt J. Lesker Company, Jefferson Hills, PA USA) via electron beam evaporation (EBE) deposition with 4N material purity minimum and a base pressure of at least 5×10^{-6} Torr. Film thickness was determined by quartz crystal monitors (QCM) and tooling factors were calibrated by measuring step height of the thin films using atomic force microscopy (AFM). The perfect absorber was fabricated using Ti and SiO_2. Other materials (Ag, Cr, Ni, Pd, Au, Al, Si, Al, TiO_2) in place of Ti for d_2 were tested for production of colored films as shown in Figure. 2(b). The hexadecimal values are extrapolated from colour averages in the images when taken at 10° from normal incidence in white fluorescent lighting. The thicknesses shown correspond to the calibrated set point of the evaporation conditions.

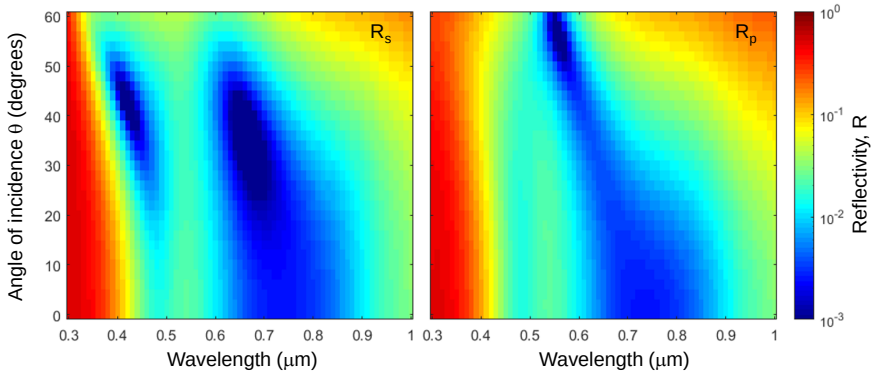

Figure 3. Plots of the simulated of reflectivity for s- and p-polarisations R_s, R_p at different angles of incidence θ within the 0.3 - 1 μm spectral window. The stack was $SiO_2/Ti/SiO_2$ with thicknesses $d_1 = 84.8$ nm, $d_2 = 7.9$ nm, $d_3 = 93.7$ nm on a 100-nm-thick Ti mirror on a soda lime glass substrate (see stack geometry in Figure. 2(a)).

Peer-reviewed version available at Micromachines 2020, 11, 256; doi:10.3390/mi11030256

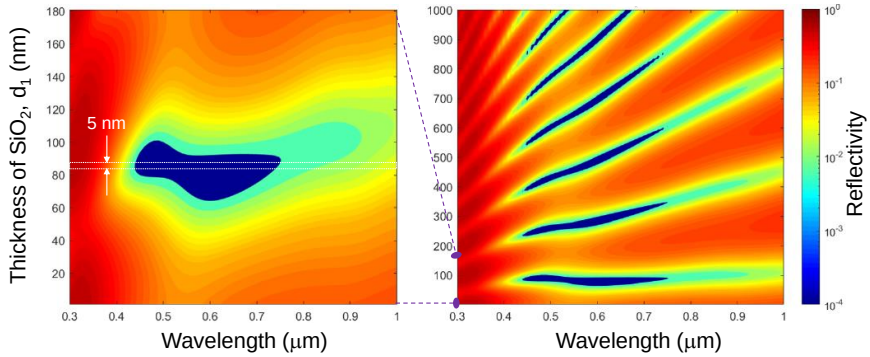

Figure 4. Plots of the simulated reflectivity R spectrum of a film stack (Figure. 2(a)) $SiO_2/Ti/SiO_2$ optical absorber, where mirror layer was Ti with $d_m = 100$ nm; note the logarithmic scale of R. Thickness of first layer SiO_2 d_1 was varied from 0 to 180 nm (left panel) to determine the minimum of R which was found at $d_1 = 84.8$ nm. The darkest blue region has ≤ 1.3 % reflectivity in the 430 - 960 nm spectral range. Other parameters: $d_2 = 7.9$ nm, $d_3 = 93.7$ nm, $d_m = 100$ nm. Normal incidence $\theta = 0°$.

3.2. Characterisation

Reflection R and transmission T of the absorber stacks were measured using a PerkinElmer 70 *Lambda 1050 WB* (Waltham, MA USA) UV-Vis-IR spectrometer. The UV spectrum is generated by a D_2 lamp (until 319.2 nm) and then a tungsten lamp is used in the Vis-IR range until 1400 nm wavelength. The UV-Vis region is detected with a photo-multiplier tube until 870 nm and then longer wavelengths are detected using an InGaAs sensor. All spectra are normalised against a 100 % Transmission, 0 % Absorbance scan inside a 150 mm integration sphere using a Labsphere Spectralon ®EPV diffuse reflectance standard (North Sutton, NH USA).

4. Results

4.1. Modeling

Multi-layer stacks of two alternating dielectrics - one dimensional photonic crystal - can achieve high reflectivity $R \to 1$ ($T \to 0$) and, ideally, without absorption losses $A = 0$. However, fabrication of such stack mirrors, usually used as spectrally narrow filters, is a formidable technical challenge due to larger number of layers $N \sim 100$. The larger the number of layers used the greater the reflectivity that can be achieved. For the opposite task, that is to obtain minimum reflectance R, multi-layer absorbers can be used.

For example, a 30-layer absorber with a 60.4 nm SiO_2 top layer with alternating layers of 10 nm Ti and decreasing thickness of SiO_2 starting from 119.6 nm down to 50 nm in steps of 2.4 nm can effectively reach $R = 1\%$ [11] (not shown here). The total thickness of such 30-layer Ti/SiO_2 stack is $\sim$2.9 µm.

In this study, further numerical optimisation was performed to reduce the total thickness whilst retaining optical impedance matching within the UV-IR spectral range. Subsequent optimisations found that a three layer stack of alternating SiO_2-Ti with thicknesses of 84.8 nm - 7.9 nm - 93.7 nm (d_1 - d_2 - d_3) on a 100-nm-thick mirror produce a similar result with a total thickness of only 386.4 nm (Figure. 2(a)).

Each of the three layers affect the reflectance R and transmittance T. The top SiO_2 (d_1) layer can only be within a certain thickness range otherwise Fresnel reflections occur at the boundary interfaces. The top three layers determine the impedance of the total system, defining which wavelengths are not reflected. The mirror layer and substrate absorbs most of the non-reflected incident light.

The effect of the first layer (d_1) thickness variation is shown in Figure. 4 where increasing Fresnel reflections causes oscillations in the spectra. Therefore the layer thickness can only be within a small range to have broadband zero reflectance ($R \to 0$). The thickness of layers two (d_2) and three (d_3) affects the optimal conditions for zero reflectance in different ways, but all layers affect the impedance

Peer-reviewed version available at Micromachines 2020, 11, 256; doi:10.3390/mi11030256

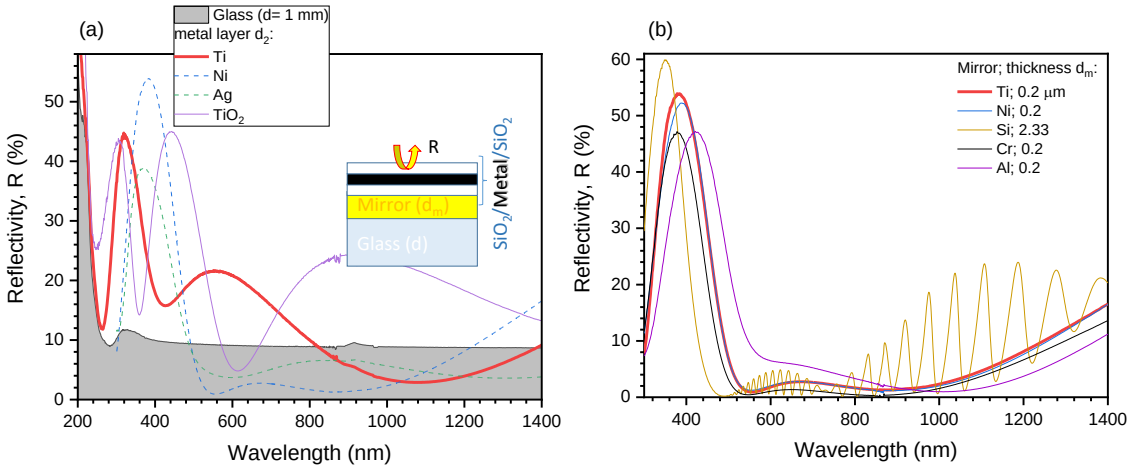

Figure 5. (a) Reflection Spectra for various d_2 materials in the when $d_2 = 7.9$ nm. A soda lime substrate reference spectra in shown in background. (b) Reflection spectra for various metals substituted as the mirror layer of $d_m = 200$ nm; for Silicon $d_m \approx 2.33$ µm (defined by evaporation time). The thickness evaluated from two interference peaks $\lambda_1 = 974.74$ nm and $\lambda_2 = 1037.11$ nm is $d_m = \frac{\lambda_1 \lambda_2}{2n(\lambda_2 - \lambda_1)} \approx 2.21$ μm calculated for the refractive index $n = 3.673$ [15].

of the absorber. The overall minimum reflectance of $R \approx 1\%$ when d_2 and d_3 varied only slightly, significant changes are evident with a 20 % thickness variation (see Appendix section for details: Figure. A1-A2). The mirror layer (d_m), by itself, is a highly lossy layer where the majority of extinction occurs; the $d_m = 100$ nm thick Ti layer on glass has transmission of $T < 1.1\%$ from 200 - 1400 nm (Figure. A3. The impedance of the incident light is wavelength dependent, thus each of the top three layers of the absorber need to vary in thickness for optimised low reflectivity performance across the spectral range considered. This is a readily achievable task and practical realisation of designed layers is shown next.

4.2. Fabrication of black-metal absorbers

The optimised thicknesses $d_{1,2,3}$ to achieve $R \to 0$ performance ($A \to 1$ perfect absorber) is outlined above in Sec. 4.1. It was established by measuring height for calibration of the metal and dielectric films deposited on patterned silicon or cover glass. This was determined outside of a clean room environment by semi-contact tapping-mode atomic force microscopy (AFM) with a 10 nm radius silicon tip. The Ti and SiO_2 films were measured to have an average surface roughness (Sa) of 0.07 nm and 1.7 nm (95 % confidence range) on silicon with peak to peak (Sy) of 0.5 nm and 20 nm respectively. The glass substrates had a measured Sa of 4.2 nm (95 % confidence range) and Sy of 62 nm. Since different metals have different surface energies, deposition of thin ~ 1 nm films is always sensitive to substrate material and its surface texture down to the nanoscale. We used e-beam evaporation and considerably high vacuum 5×10^{-6} Torr which facilitates formation of smooth layers of high purity. The surface roughness of titanium metal used in this study deposited on silicon for thickness calibration was $\Delta d = \pm 0.25$ nm ($\frac{1}{2}Sy$) over the length of ~ 5 μm. Thickness of the deposited films is given by the quartz micro-balance method from the linear fit mass vs time at the chosen deposition rate (conditions). Precision of such method was ± 0.1 nm where the most significant process control is from tooling of the quartz micro-balance. The second process control taken into account is a read delay of the quartz micro-balance. The shutter closes once the thickness set point is reached but due to continuous read-out there is a delay (as well as temperature drop) of the actual thickness. The thickness overshoot was found to have a linear relationship with deposition rate for each material. Precision of film deposition thickness read out by the crystal monitor was $\Delta d = 0.1$ nm (defined as a mass of the deposited film) over multiple deposition runs. Therefore the total thickness margin of error from the deposition is $\Delta d = 0.35$ nm.

Peer-reviewed version available at Micromachines 2020, 11, 256; doi:10.3390/mi11030256

The designed Ti nano-layer structure (Figure. 2(a)) was fabricated. Reflectance spectrum (Figure. 5(a)) sharply decreases at the wavelengths longer than 400 nm as in the simulated spectrum Figure. 4. The actual thickness d_2 (Ti) was most probably less than the simulated by ~ 1 nm, which can explain the higher reflectivity and saddle shape around 600 nm wavelength as shown in simulations Figure. A1. Reflectance R becomes smaller than 0.1 of the glass only at around 800 nm. Since the structure is made on a 100-nm-thick Ti mirror, a close to 90% reflectance is expected. For example, the $d = 100$ nm thickness of Au should reduce transmission to $T = e^{-\alpha d} \equiv e^{-(4\pi\kappa/\lambda)d} = 0.11\%$, here the absorption coefficient α is expressed via the extinction coefficient κ (the complex refractive coefficient $(n + i\kappa)$), which has value of $\kappa = 3.4332$ for wavelength $\lambda = 633$ nm [16].

Low reflectance for the Ag and Ni layers over the 500 - 1200 nm spectral window was observed in fabricated three-layer films on Ti-mirror (Figure. 5(a)). The reflectance of the glass in the 500 - 1400 nm range is 8.9%. The Ti d_2 layer sample has a reduced reflectance in the 821 - 1385 nm range but is greater below 821 nm and has an overall reflectance of 9.3% in the 500 - 1400 nm range, thus, the layer thicknesses require further optimisation to match simulations. Similarly, for the Ag d_2 and the Ni d_2 samples, reflectance in the 500 - 1400 nm range are 4.9% (minimum 3.6% @ 1307 nm) and 4.9% (minimum 0.9% @ 556 nm) respectively, reducing reflectance to 55.1 and 54.9% to that of glass respectively.

Noteworthy, the structure was not simulated nor optimised for Ag and Ni and was deposited for comparison as not impedance matched structures. Figure. 2(b) shows appearance of the black-metal mirrors whose reflectance is presented in Figure. 5(a). Titania (TiO_2) was also tested as layer-2 since Ti can be oxidised after exposure to room conditions and the SiO_2 layers. Strong reflectivity around 400 nm (3.1 eV) was observed. This is consistent with band-gap edge absorption of titania. At the strong absorption, low reflectivity $R = 1 - A - T$ is expected when $T \to 0$ as in the studied case.

The influence of the mirror-layer (originally 100 nm of Ti) was tested by evaporating films of different materials (Figure. 5(b)); the optimised Ti structure is shown in Figure. 2(a). The reflectivity is considerably lower than that of cover glass. Different metals behaved similarly with strongest difference at the UV spectral range where free-electron density differences become important. Interestingly, a 2.3 μm Si showed similar performance up to 900 nm wavelengths (close to the absorption band-gap of 1.12 eV). The best performance of a low $R < 4\%$ reflection was obtained with the $SiO_2/Ti/SiO_2$ designed structure but on a Ti-mirror of $d_m = 200$ nm thickness (Figure. 5(b)). Its low reflectivity spanned the 500-1000 nm spectral band.

5. Discussion

It is usual to expect that metal coatings are reflective mirrors. Here we show that nano-engineered silica-metal-silica layers deposited on a mirror renders its surface black (dark) and delivers a low reflectance $R \to 0$.

Simulations and experimental spectra have variation differences quantitatively but agree well qualitatively for the expected reflectivity spectral line shape. Exact layer thicknesses are yet to be achieved as detailed in Figure. 5 (a) as the minimum reflectance achieved is with a nickel d_2 layer Fabrication error is on the order of ± 0.35 nm due to thin film grain formation and lateral uniformity of the film even when the quartz micro-balance tooling accuracy defining mass is ± 0.1 nm. Across multiple deposition runs tested experimentally, thickness variation accuracy remains to within 0.1 nm although the overall thickness error is larger due to grain formation. Step height measurements using AFM are accurate, however, a change in interface profile when a layer is deposited over the top is not well known.

Material of the mirror-layer had minimal effect on the reflection spectra, oxidation of the mirror at the interface with the SiO_2 will occur for the reactive metals. Oxidation of a thin nanometer-scale Ti layer can have influence on the optical constants $(n + i\kappa)$. Moreover, we have demonstrated that when thickness of sputtered films is ~ 10 nm, the nanoscale roughness has a strong influence and optical performance of metamaterial absorbers at IR spectral window departs from numerical predictions based on optical constants [17]. By invoking surface roughness at the interface and top surface, it was possible to obtain more closely matching transmission spectra [17]. Future work is necessary to reach more quantitative match between theory and experiment and will be carried out in the nearest future.

Peer-reviewed version available at Micromachines 2020, 11, 256; doi:10.3390/mi11030256

6. Conclusions and Outlook

Reflectivity of “black-metals" lower than that of glass over the spectral range of 500 - 1000 nm can be made by a simple silica-metal-silica sandwich deposited over a back-reflecting mirror. Glass was measured to have a broadband reflectance of ~ 8.9 % (>400 nm) and the impedance matched layers are able to reduce reflectance in comparison. The broadband reflectance from 500 - 1400 nm values measured for d_2 layer materials are Ti: 9.3%, Ag: 4.9% and Ni: 4.9%. Mirror material was not the most critical parameter for the spectral bandwidth. Thickness of a thin metal film of the second layer $d_2 \approx 8$ nm is the most sensitive parameter defining the reflection spectrum. Considerable departure of spectral response of the fabricated structure from that simulated is attributed to imperfections at the interface regions as previously observed for IR metamaterial absorbers [17]. Further optimisations of film thickness accuracy will produce optimal results for a zero reflectance ($R \to 0$) optical metamaterial.

Fabrication of thin films with a specific optical function and making them chemically releasable for opto-mechanical manipulation [18] could also be used for metamaterial coatings studied in this work. How the low emissivity of metals ($0.02 - 0.05$) as compared to that of black-body (emissivity of 1) is changed for the antireflective black-metal surfaces is the next intriguing quest. Following the experimentally demonstrated Kirchhoff’s law for IR metamaterial absorbers, when a strong absorbance at a spectrally narrow IR band showed the proportional emittance $E \approx A$ [19], the expectation is that silica-metal-silica structures on a mirror would be a broad band thermal emitter.

Author Contributions: Conceptualization, M.M and S.J.; methodology, S.L; S.H.N. validation, S.L. and M.M.; investigation, S.L., S.H.N. and Y.N.; visualization, S. L.; writing–original draft preparation, S.L.; writing–review and editing, all the authors.

Funding: This research was funded by the Melbourne University administrated DSI-RHD 2018, ARC Discovery DP190103284, Linkage LP190100505 grants, and EPSRC EP/M000869/1.

Acknowledgments: We acknowledge support via strategic operational funding of the Nanotechnology facility at Swinburne University.

Conflicts of Interest: The authors declare no conflict of interest.

Appendix A Parameter study of: 1) d_1 dependence on $d_{2,3}$ and 2) d_m

Effect of the second layer, Ti thickness variation shown in Figure. A1. The layer thickness was varied by 2 nm ($\sim$ 20% of the layer thickness) and the third layer, SiO_2 impact heavily the impedance of the system and define where the zero reflectance region occurs along the optical spectrum. By increasing layer-3 (SiO_2) thickness, the zero reflection region will red-shift and a greater fraction of the IR spectrum will not be reflected, but more of the UV-Vis spectrum will be reflected. The reverse is true when the layer-3 thickness is decreased, blue shifting the zero reflectance region as shown in Figure. A2. Figure A3 shows the experimentally measured overall transmittance (at normal incidence) for different Ti thicknesses. The integrated total transmittance over the measured spectral window is also shown as a percentage value.

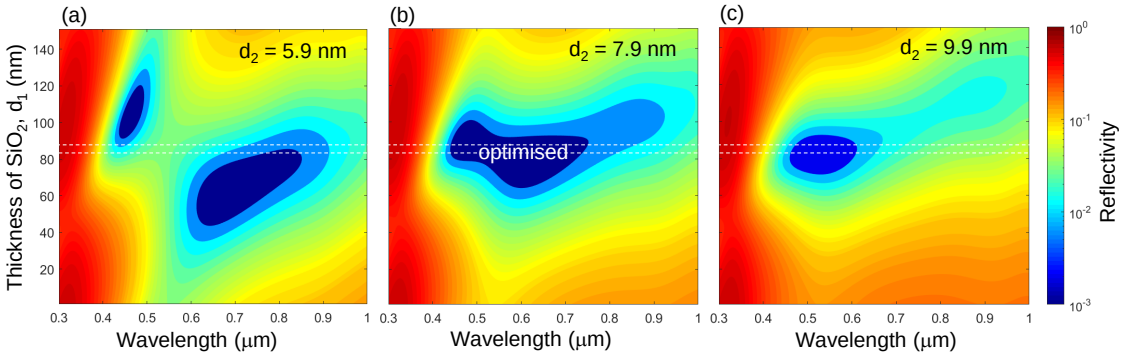

Figure A1. Simulations of the d_1 SiO_2 effect on the performance of $SiO_2/Ti/SiO_2$ layers where layer-2 (Ti) was $d_2 = 5.9$ nm (a), $d_2 = 7.9$ nm (b) and $d_2 = 9.9$ nm (c) thick (structure is shown in Figure. 2(a)); thickness $d_3 = 93.7$ nm. Normal incidence $\theta = 0°$.

Peer-reviewed version available at Micromachines 2020, 11, 256; doi:10.3390/mi11030256

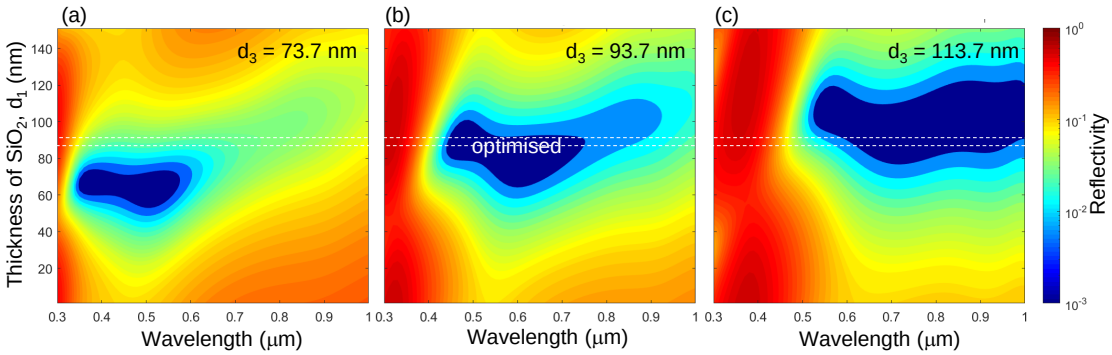

Figure A2. Simulations of the d_1 and d_3 SiO_2 thickness effect on the performance of $SiO_2/Ti/SiO_2$ layers. Layer-3 (SiO_2) is varied in steps of 20 nm: $d_3 = 73.7$ nm (a), $d_3 = 93.7$ nm (b) and $d_3 = 113.7$ nm (c); structure is shown in Figure. 2(a); thickness $d_2 = 7.9$ nm. Normal incidence $\theta = 0°$.

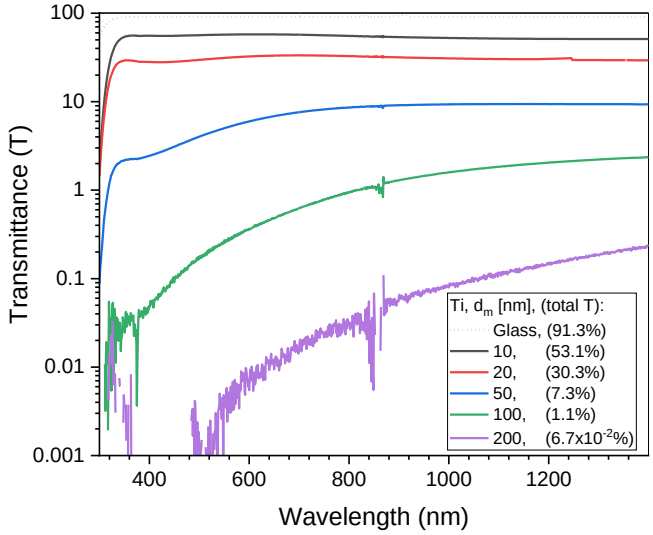

Figure A3. Titanium mirror layer (d_m) thickness effect on the transmittance of incident light. Total integral transmittance T [%] is calculated from area under the curve.

1. Yu, N.; Capasso, F. Flat Optics with Designer Metasurfaces. *Nature materials* **2014**, *13*, 139–150. doi:10.1038/nmat3839.
2. Kats, M.A.; Capasso, F. Optical absorbers based on strong interference in ultra-thin films. *Laser and Photonics Reviews* **2016**, *10*, 735–749, [1606.05707]. doi:10.1002/lpor.201600098.
3. Holloway, C.L.; Kuester, E.F.; Gordon, J.A.; O'Hara, J.; Booth, J.; Smith, D.R. An Overview of the Theory and Applications of Metasurfaces: The Two-Dimensional Equivalents of Metamaterials. *IEEE Antennas and Propagation Magazine* **2012**, *54*, 10–35. doi:10.1109/MAP.2012.6230714.
4. Zheludev, N.I.; Kivshar, Y.S. From metamaterials to metadevices. *Nature Materials* **2012**, *11*, 917–924. doi:10.1038/nmat3431.
5. El-Ganainy, R.; Makris, K.G.; Christodoulides, D.N.; Musslimani, Z.H. Theory of Coupled Optical PT-Symmetric Structures. *Optics Letters* **2007**, *32*, 2632. doi:10.1364/ol.32.002632.
6. Özdemir, K.; Rotter, S.; Nori, F.; Yang, L. Parity–Time Symmetry and Exceptional Points in Photonics. *Nature Materials* **2019**, *18*, 783–798. doi:10.1038/s41563-019-0304-9.
7. Dharmavarapu, R.; Ng, S.H.; Eftekhari, F.; Juodkazis, S.; Bhattacharya, S. MetaOptics: opensource software for designing metasurface optical element GDSII layouts. *Opt. Express* **2020**, *28*, 3505–3516.

8. Beranek, L.L.; Sleeper, H.P. The Design and Construction of Anechoic Sound Chambers. *Journal of the Acoustical Society of America* **1946**, *18*, 140–150. doi:10.1121/1.1916351.
9. Liu, N.; Mesch, M.; Weiss, T.; Hentschel, M.; Giessen, H. Infrared perfect absorber and its application as plasmonic sensor. *Nano Letters* **2010**, *10*, 2342–2348, [arXiv:1011.1669v3]. doi:10.1021/nl9041033.
10. Matthaei, G.L.; Young, L.; Jones, E. *Microwave Filters, Impedance Inverters and Coupling Structures*; McGraw-Hill Book Company, Inc.: Norwood, MA 02062, 1964; p. 1096.
11. Mazilu, M.; Dholakia, K. Optical impedance of metallic nano-structures. *Optics Express* **2006**, *14*, 7709. doi:10.1364/oe.14.007709.
12. Noh, H.; Chong, Y.; Stone, A.D.; Cao, H. Perfect coupling of light to surface plasmons by coherent absorption. *Physical Review Letters* **2012**, *108*, 1–5. doi:10.1103/PhysRevLett.108.186805.
13. Valentine, J.; Zhang, S.; Zentgraf, T.; Ulin-Avila, E.; Genov, D.A.; Bartal, G.; Zhang, X. Three-dimensional optical metamaterial with a negative refractive index. *Nature* **2008**, *455*, 376–379. doi:10.1038/nature07247.
14. Refractive index database. Online accessed 26 jan 2020 https://refractiveindex.info/. (Accessed: 26 January 2020).
15. Aspnes, D.; A.A.Studna. Dielectric functions and optical parameters of Si,Ge,GaP,GaAs,GaSb,InP,InAs and InSb from 1.5 to 6.0 eV. *Physical Review B* **1983**, *27*.
16. P. B. Johnson and R. W. Christy. Optical Constant of the Nobel Metals. *Physical Review B* **1972**, *6*, 4370–4379.
17. Nishijima, Y.; Balčytis, A.; Naganuma, S.; Seniutinas, G.; Juodkazis, S. Tailoring Metal and Insulator Contributions in Plasmonic Perfect Absorber Metasurfaces. *ACS Applied Nano Materials* **2018**, *1*, 3557–3564. doi:10.1021/acsanm.8b00710.
18. Grineviciute, L.; Tolenis, T.; Ryu, M.; Moein, T.; Ng, S.H.; Katkus, T.; Maksimovic, J.; Drazdys, R.; Morikawa, J.; Juodkazis, S. Releasable Micro-Waveplates. *arXiv preprint* **2019**, pp. 2–5, [1907.05485].
19. Nishijima, Y.; Balčytis, A.; Naganuma, S.; Seniutinas, G.; Juodkazis, S. Kirchhoff's Metasurfaces Towards Efficient Photo-Thermal Energy Conversion. *Scientific Reports* **2019**, *9*, 1–9. doi:10.1038/s41598-019-44781-4.